Transport properties of an Aharonov–Bohm ring with strong interdot Coulomb interaction

2007 J. Phys.: Condens. Matter 19 246201

(http://iopscience.iop.org/0953-8984/19/24/246201)

IOP PUBLISHING JOURNAL OF PHYSICS: CONDENSED MATTER

J. Phys.: Condens. Matter **19** (2007) 246201 (16pp) doi:10.1088/0953-8984/19/24/246201

Transport properties of an Aharonov–Bohm ring with strong interdot Coulomb interaction

Yu-Shen Liu[1,2], **Hao Chen**[1,4] **and Xi-Feng Yang**[3]

[1] Physics Department, Fudan University, Shanghai 200433, People's Republic of China
[2] Physics Department, Qufu Normal University, Qufu 273165, People's Republic of China
[3] National Lab for Infrared Physics, Shanghai Institute of Technical Physics, Chinese Academy of Sciences, 500 Yutian Road, Shanghai 200083, People's Republic of China

E-mail: haochen@fudan.edu.cn

Received 1 February 2007, in final form 15 April 2007
Published 17 May 2007
Online at stacks.iop.org/JPhysCM/19/246201

Abstract

Based on the Keldysh Green's function technique and the equation-of-motion method, we investigate theoretically the electronic transport properties of an Aharonov–Bohm ring with embedded coupled double quantum dots connected to two electrodes in a symmetrical parallel configuration in the presence of strong interdot Coulomb interaction. Special attention is paid to the effects of the interdot Coulomb interaction on the transport properties. It has been shown numerically that the interdot Coulomb interaction gives rise to four electronic states in the ring. The quantum interferences between two strongly coupled electronic states and two weakly coupled ones lead to two Breit–Wigner and two Fano resonances in the linear conductance spectrum with the magnetic flux switched on or the imbalance between the energy levels of two quantum dots. The positions and shapes of the four resonances can be controlled by adjusting the magnetic flux through the device or energy levels of the two quantum dots. When the Fermi energy levels in the leads sweep across the weakly coupled electronic states, the negative differential conductance (NDC) is developed in the current–voltage characteristics for the non-equilibrium case.

(Some figures in this article are in colour only in the electronic version)

1. Introduction

Electronic transport through mesoscopic systems such as a quantum dot (QD) or molecular systems with geometrical dimensions smaller than the elastic mean free paths has been an active research subject due to the advances in the nanofabrication of quantum devices in recent years [1–4]. In such mesoscopic systems, the electronic transport is ballistic, while the phase coherence is preserved. In particular, a double quantum dot connected to the source and to

[4] Author to whom any correspondence should be addressed.

the drain electrodes, either in series or parallel configurations, has been extensively studied experimentally and theoretically [5–15], mainly because of its potentials for fundamental physical studies as well as for applications for future quantum communication techniques.

Holleitner *et al* [16] proposed a quantum device with two coupled quantum dots embedded in an Aharonov–Bohm ring, and a flux-periodic current was detected for weakly coupled quantum dots. Kobayashi *et al* [17] presented a quantum interference experiment with a quantum dot embedded in an Aharonov–Bohm ring fabricated in a two dimensional AlGaAs/GaAs heterostructure, and they gave a convincing demonstration of the Fano effect in a mesoscopic system. The well known Fano effect is a result of the quantum interference between the resonance state and the continuum state, and is a powerful tool to study the electron phase variation in QD systems. In addition to some experimental works, there has been theoretical work on an electron through a double quantum-dot molecule connected in a parallel configuration to the leads [7]. The system is modelled by means of a non-interacting two-site Anderson Hamiltonian. In general the conductance spectrum is composed of Breit–Wigner and Fano line shapes at the bonding and antibonding states, respectively. Recently, coherent electronic transport through a double quantum dot system connected in series with two leads has been studied by Bulka *et al* [18], in which electron correlation effects are treated. More recently, Meden *et al* [19] investigated electronic transport through parallel DQDs with electron–electron correlations at different sites by using the numerical renormalization group technique at zero temperature. Their results show that the correlations generate resonances in electronic transport. However, the non-equilibrium cases with the appearance of the negative differential conductance have not been considered in [19]. Kuo *et al* [20] investigated charge transport through parallel double single electron transistors (SETs) with the interdot Coulomb repulsion in the absence of the Fano effect where the two SETs do not couple to each other through the two leads. Lu *et al* [21] studied the Fano effect through parallel-coupled DQDs in the presence of on-dot Coulomb correlation without the interdot Coulomb interaction.

Recently, the double quantum dot system has become of special interest for quantum computation as a basic unit of information, a qubit, because the entanglement of electrons can be generated in a controllable manner [22]. For example, the two coupled quantum dots always form bonding and antibonding states like a molecule of two atoms. This opens the possibility for realistic applications of quantum computers [23–25]. In this paper we study electronic transport through DQDs including the interdot Coulomb interaction within the Keldysh Green's function technique. The DQDs are attached to the two external leads in a parallel configuration. Numerical results show that the strong interdot Coulomb interaction opens new resonant channels across the device. As a result of the quantum interference effect of the electronic transition through the weakly coupled and strongly coupled electronic states, the linear conductance spectrum is often composed of two Breit–Wigner resonances and two Fano resonances when the magnetic field is threading the ring or the finite energies difference of the two quantum dots is presented for the symmetrical coupling system. These electronic states can be controlled by adjusting the parameters of the system. The non-equilibrium case is also studied in this paper. We find that the negative differential conductance (NDC) occurs when the applied voltage sweeps across the weakly coupled electronic states and the difference between the numbers of electrons occupying the two quantum dots changes drastically.

2. Physical model

The configuration consists of two single-level coupled quantum dots attached in a parallel configuration to the leads as schematically shown in figure 1. The total magnetic flux $(\Phi_L+\Phi_R)$ is applied perpendicular to the structure, which provides the Aharonov–Bohm phase-shift

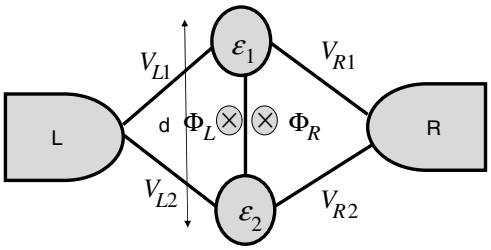

Figure 1. Schematic plot of the double coupled quantum dots coupled in a symmetrical parallel configuration to the left and right leads. Φ_L threads through the left sub-ring and Φ_R threads through the right sub-ring.

between the electron waves propagating in the clockwise and anticlockwise directions. The quantum system is modelled by the following Hamiltonian:

$$H_{\text{total}} = H_{\text{leads}} + H_{\text{DQD}} + H_{\text{T}}, \tag{1}$$

where H_{leads} describes the two leads in the noninteracting quasiparticle approximation,

$$H_{\text{leads}} = \sum_{k,\nu=L,R} \epsilon_{k\nu} a^{\dagger}_{k\nu} a_{k\nu}, \tag{2}$$

and $a^{\dagger}_{k\nu}$ ($a_{k\nu}$) creates (destroys) an electron with the single-electron energy $\epsilon_{k\nu}$ and momentum $\hbar k$ in lead $\nu(\nu = L, R)$. When the external bias voltage V is applied across the mesoscopic system, the chemical potential difference between the two leads becomes $\mu_L - \mu_R = eV$. H_{DQD} describes the dynamics of the coupled double dots with interdot interaction U

$$H_{\text{DQD}} = \sum_{j=1,2} \epsilon_j d^{\dagger}_j d_j + U d^{\dagger}_1 d_1 d^{\dagger}_2 d_2 - t_{\text{c}} \mathrm{e}^{\mathrm{i}\theta} d^{\dagger}_1 d_2 - t^{*}_{\text{c}} \mathrm{e}^{-\mathrm{i}\theta} d^{\dagger}_2 d_1, \tag{3}$$

where $d^{\dagger}_j(d_j)$ $(j = 1, 2)$ creates (destroys) an electron with the bare energy level ϵ_j in dot j, and t_{c} denotes the inter-dot tunnelling coupling. This is valid when the sizes of the two quantum dots are small; only one energy level is active in each quantum dot [26, 27]. The interdot Coulomb interaction is included, $U = \mathrm{e}^2/\varepsilon\,\mathrm{d}$, with the dielectric constant ε and the quantum dots distance d. The interdot H_{T} models the tunnelling among the coupled double dots and the two leads

$$H_{\text{T}} = \sum_{k,\nu=L,R} [(V_{\nu 1} d^{\dagger}_1 + V_{\nu 2} d^{\dagger}_2) a_{k\nu} + \text{H.c}]. \tag{4}$$

By assuming the energy independence of the tunnelling coupling among the double dots and the leads, the tunnelling matrix elements can be written as $V_{L1} = |V_{L1}|\mathrm{e}^{\mathrm{i}\phi/4}$, $V_{L2} = |V_{L2}|\mathrm{e}^{-\mathrm{i}\phi/4}$, $V_{R1} = |V_{R1}|\mathrm{e}^{-\mathrm{i}\phi/4}$, and $V_{R2} = |V_{R2}|\mathrm{e}^{\mathrm{i}\phi/4}$, with the AB phase $\phi = 2\pi(\Phi_L + \Phi_R)/\Phi_0$ and the flux quantum $\Phi_0 = hc/e$. The left sub-ring of the AB ring is threaded by the flux Φ_L and the right sub-ring of the AB ring is threaded by the flux Φ_R. The magnetic flux imbalance θ is expressed by the difference of Φ_R and Φ_L, $\theta = \pi(\Phi_R - \Phi_L)/\Phi_0$, where the contribution from the phases of $V_{\nu,i}$ is cancelled [8, 10]. In the presence of the magnetic flux, the linewidth matrices Γ^L and Γ^R can be expressed as

$$\Gamma^L = \begin{pmatrix} \Gamma^L_1 & \sqrt{\Gamma^L_1 \Gamma^L_2}\,\mathrm{e}^{\mathrm{i}\phi/2} \\ \sqrt{\Gamma^L_1 \Gamma^L_2}\,\mathrm{e}^{-\mathrm{i}\phi/2} & \Gamma^L_2 \end{pmatrix}, \tag{5}$$

and

$$\Gamma^R = \begin{pmatrix} \Gamma^R_1 & \sqrt{\Gamma^R_1 \Gamma^R_2}\,\mathrm{e}^{-\mathrm{i}\phi/2} \\ \sqrt{\Gamma^R_1 \Gamma^R_2}\,\mathrm{e}^{\mathrm{i}\phi/2} & \Gamma^R_2 \end{pmatrix}, \tag{6}$$

with the linewidth matrix $\Gamma^{\nu}_j = \sum_k |V_{\nu j}|^2 2\pi\delta(\epsilon - \epsilon_{k\nu})$, $(j = 1, 2)$.

3. Green's function of the two dots

In order to study the transport behaviour of the device shown in figure 1, we utilize the Keldysh Green's function of the two dots. First, we consider two coupled quantum dots as a 'dimer', and perform a unitary transformation to $H_{\rm DQD}$ in the basis of the bonding and antibonding states [10, 28]

$$d_1 = \cos\beta \mathrm{e}^{\mathrm{i}\theta} f_+ + \sin\beta f_- \tag{7}$$

and

$$d_2 = -\sin\beta f_+ + \cos\beta \mathrm{e}^{-\mathrm{i}\theta} f_-, \tag{8}$$

with parameter β defined as

$$\beta = \frac{1}{2}\tan^{-1}\frac{2t_{\rm c}}{\epsilon_1 - \epsilon_2}. \tag{9}$$

The Hamiltonian of the isolated quantum dot molecule is expressed as

$$\overline{H}_{\rm DQD} = \epsilon_+ f_+^\dagger f_+ + \epsilon_- f_-^\dagger f_- + U f_+^\dagger f_+ f_-^\dagger f_-, \tag{10}$$

with

$$\epsilon_\pm = \tfrac{1}{2}[\epsilon_1 + \epsilon_2 \pm \sqrt{(\epsilon_1 - \epsilon_2)^2 + 4t_{\rm c}^2}], \tag{11}$$

where $f_{+(-)}^\dagger$ is the creation operator for the bonding (antibonding) state of the two-dot set-up. In terms of the new Fermi operator, the tunnelling Hamiltonian among the two leads and DQD is written as

$$\overline{H}_{\rm T} = \sum_{k,\nu=L,R}\{(\overline{V}_{\nu+} f_+^\dagger + \overline{V}_{\nu-} f_-^\dagger)a_{k\nu} + \text{H.c.}\}, \tag{12}$$

with the effective tunnelling matrix elements

$$\overline{V}_{\nu+} = V_{\nu 1}\cos\beta \mathrm{e}^{-\mathrm{i}\theta} - V_{\nu 2}\sin\beta, \tag{13}$$

$$\overline{V}_{\nu-} = V_{\nu 1}\sin\beta + V_{\nu 2}\cos\beta \mathrm{e}^{\mathrm{i}\theta}. \tag{14}$$

The Hamiltonian of the whole system can be rewritten as

$$\begin{aligned}\tilde{H}_{\rm total} = &\sum_{k,\nu=L,R}\epsilon_{k\nu}a_{k\nu}^\dagger a_{k\nu} + \epsilon_+ f_+^\dagger f_+ + \epsilon_- f_-^\dagger f_- + U f_+^\dagger f_+ f_-^\dagger f_- \\ &+ \sum_{k,\nu=L,R}\{(\overline{V}_{\nu+} f_+^\dagger + \overline{V}_{\nu-} f_-^\dagger)a_{k\nu} + \text{H.c.}\}.\end{aligned} \tag{15}$$

The DQD retarded, advanced Green's functions for the two molecular states are defined in the time space as

$$G_{\alpha\beta}^r(t,t') = -\mathrm{i}\Theta(t-t')\langle\{f_\alpha(t), f_\beta^\dagger(t')\}\rangle, \tag{16}$$

$$G_{\alpha\beta}^a(t,t') = \mathrm{i}\Theta(t'-t)\langle\{f_\alpha(t), f_\beta^\dagger(t')\}\rangle, \tag{17}$$

and the lesser Green's function is written

$$G_{\alpha\beta}^<(t,t') = \mathrm{i}\langle f_\alpha^\dagger(t') f_\beta(t)\rangle, \qquad (\alpha,\beta = \pm) \tag{18}$$

where $\Theta(t)$ is the step function; bracket $\langle\cdot\rangle$ represents the statistical average. The above Green's functions only depend on the variable $\Delta t = t - t'$ when all calculations are limited to the steady state. In order to calculate the current through the device, we have to know the expressions of the retarded and lesser Green's functions of the total system including two leads and two coupled dots. In the following, we shall derive the retarded Green's function $G_{\alpha\beta}^r(\epsilon) = \langle\langle f_\alpha \mid f_\beta^\dagger\rangle\rangle_\epsilon^r$, which is the Fourier transform of equation (16). Using the standard

equation-of-motion technique $\epsilon\langle\langle f_\alpha|f_\beta^\dagger\rangle\rangle_\epsilon^r = \langle\{f_\alpha, f_\beta^\dagger\}\rangle + \langle\langle[f_\alpha, \tilde{H}_{\rm total}]|f_\beta^\dagger\rangle\rangle_\epsilon^r$, we arrive at the following equation:

$$(\epsilon-\epsilon_\alpha)\langle\langle f_\alpha \mid f_\beta^\dagger\rangle\rangle_\epsilon^r = \delta_{\alpha\beta} + U\langle\langle f_\alpha f_{\overline{\alpha}}^\dagger f_{\overline{\alpha}}|f_\beta^\dagger\rangle\rangle_\epsilon^r + \sum_{k,\nu}\overline{V}_{\nu\alpha}\langle\langle a_{k\nu}|f_\beta^\dagger\rangle\rangle_\epsilon^r, \tag{19}$$

where $\overline{\alpha} = +$ for $\alpha = -$ and $\overline{\alpha} = -$ for $\alpha = +$. Two new Green's functions appear on the right side of equation (19). $\langle\langle a_{k\nu}|f_\beta^\dagger\rangle\rangle_\epsilon^r$ is generated by the hopping between the two quantum dots and the two leads, which can be expressed by using the Dyson equation

$$\langle\langle a_{k\nu}|f_\beta^\dagger\rangle\rangle_\epsilon^r = \overline{V}_{\nu\alpha}^* g_{k\nu}^r\langle\langle f_\alpha|f_\beta^\dagger\rangle\rangle_\epsilon^r + \overline{V}_{\nu\overline{\alpha}}^* g_{k\nu}^r\langle\langle f_{\overline{\alpha}}|f_\beta^\dagger\rangle\rangle_\epsilon^r, \tag{20}$$

where $g_{k\nu}^r$ is the free-electron retarded Green's function in the two leads with the relations $g_{k\nu}^r = 1/(\epsilon-\epsilon_{k\nu}+{\rm i}0^+)$. $\langle\langle f_\alpha f_{\overline{\alpha}}^\dagger f_{\overline{\alpha}}|f_\beta^\dagger\rangle\rangle_\epsilon^r$ is the two-particle Green's function generated by the interdot interaction term in equation (3). Using the standard equation-of-motion technique for it, we obtain

$$\begin{aligned}(\epsilon-\epsilon_\alpha-U)\langle\langle f_\alpha f_{\overline{\alpha}}^\dagger f_{\overline{\alpha}}|f_\beta^\dagger\rangle\rangle_\epsilon^r &= \langle\{f_\alpha f_{\overline{\alpha}}^\dagger f_{\overline{\alpha}}, f_\beta^\dagger\}\rangle + \sum_{k\nu}\{\overline{V}_{\nu\alpha}\langle\langle a_{k\nu}f_{\overline{\alpha}}^\dagger f_{\overline{\alpha}}|f_\beta^\dagger\rangle\rangle_\epsilon^r \\ &\quad - \overline{V}_{\nu\overline{\alpha}}^*\langle\langle f_\alpha a_{k\nu}^\dagger f_{\overline{\alpha}}|f_\beta^\dagger\rangle\rangle_\epsilon^r + \overline{V}_{\nu\overline{\alpha}}\langle\langle f_\alpha f_{\overline{\alpha}}^\dagger a_{k\nu}|f_\beta^\dagger\rangle\rangle_\epsilon^r\}.\end{aligned} \tag{21}$$

Three higher-order Green's functions appear on the right of equation (21). In this paper, we employ the Hartree–Fock approximation for the higher-order Green's functions [29–31], which is valid at temperatures higher than the Kondo temperature. Kashcheyevs *et al* [32], who studied the Kondo effect at zero temperature, showed that this model can be exactly mapped onto a generalized Anderson model and the Kondo temperature $T_{\rm K}$ is given as that in a single quantum dot. The Kondo temperature was found to be lower than the bath temperature in the experiment [16], where the quantum dots are weakly coupled to the leads.

$$\langle\langle a_{k\nu}f_{\overline{\alpha}}^\dagger f_{\overline{\alpha}}|f_\beta^\dagger\rangle\rangle_\epsilon^r \sim \langle f_{\overline{\alpha}}^\dagger f_{\overline{\alpha}}\rangle\langle\langle a_{k\nu}|f_\beta^\dagger\rangle\rangle_\epsilon^r, \tag{22}$$

$$\langle\langle f_\alpha f_{\overline{\alpha}}^\dagger a_{k\nu}|f_\beta^\dagger\rangle\rangle_\epsilon^r \sim -\langle f_{\overline{\alpha}}^\dagger f_\alpha\rangle\langle\langle a_{k\nu}|f_\beta^\dagger\rangle\rangle_\epsilon^r, \tag{23}$$

and

$$\langle\langle f_\alpha a_{k\nu}^\dagger f_{\overline{\alpha}}|f_\beta^\dagger\rangle\rangle_\epsilon^r \sim 0. \tag{24}$$

Flip processes between the bonding state ('+') and antibonding state ('−') are considered as shown in equation (23). Substituting equations (22)–(24) into equation (21) and combining equations (19) and (20), the two linear equations are obtained:

$$\begin{aligned}&[1-g_{\alpha\alpha}^r(\epsilon)\bar{\Sigma}_{\alpha\alpha}^r(\epsilon) - g_{\alpha\bar{\alpha}}^r(\epsilon)\bar{\Sigma}_{\bar{\alpha}\alpha}^r(\epsilon)]G_{\alpha\alpha}^r(\epsilon) = g_{\alpha\alpha}^r(\epsilon) \\ &\qquad + [g_{\alpha\alpha}^r(\epsilon)\bar{\Sigma}_{\alpha\bar{\alpha}}^r(\epsilon) + g_{\alpha\bar{\alpha}}^r(\epsilon)\bar{\Sigma}_{\bar{\alpha}\bar{\alpha}}^r(\epsilon)]G_{\bar{\alpha}\alpha}^r(\epsilon),\end{aligned} \tag{25}$$

$$\begin{aligned}&[1-g_{\bar{\alpha}\bar{\alpha}}^r(\epsilon)\bar{\Sigma}_{\bar{\alpha}\bar{\alpha}}^r(\epsilon) - g_{\bar{\alpha}\alpha}^r(\epsilon)\bar{\Sigma}_{\alpha\bar{\alpha}}^r(\epsilon)]G_{\bar{\alpha}\alpha}^r(\epsilon) = g_{\bar{\alpha}\alpha}^r(\epsilon) \\ &\qquad + [g_{\bar{\alpha}\bar{\alpha}}^r(\epsilon)\bar{\Sigma}_{\bar{\alpha}\alpha}^r(\epsilon) + g_{\bar{\alpha}\alpha}^r(\epsilon)\bar{\Sigma}_{\alpha\alpha}^r(\epsilon)]G_{\alpha\alpha}^r(\epsilon),\end{aligned} \tag{26}$$

where $g_{\alpha\alpha}^r(\epsilon) = \frac{1-\langle f_{\bar{\alpha}}^\dagger f_{\bar{\alpha}}\rangle}{\epsilon-\epsilon_\alpha+{\rm i}0^+} + \frac{\langle f_{\bar{\alpha}}^\dagger f_{\bar{\alpha}}\rangle}{\epsilon-\epsilon_\alpha-U+{\rm i}0^+}$ denotes diagonal elements of the retarded Green's function of two coupled dots without the connection to the leads, in which there are two resonances located in the vicinity of $\epsilon = \epsilon_\alpha$ and $\epsilon = \epsilon_\alpha + U$, with corresponding weights $1-\langle f_{\bar{\alpha}}^\dagger f_{\bar{\alpha}}\rangle$ and $\langle f_{\bar{\alpha}}^\dagger f_{\bar{\alpha}}\rangle$, respectively. Here $n_{\bar{\alpha}} = \langle f_{\bar{\alpha}}^\dagger f_{\bar{\alpha}}\rangle$ is the occupied number in state $\bar{\alpha}$ of the quantum dot molecule. $g_{\bar{\alpha}\alpha} = -\frac{\langle f_\alpha^+ f_{\bar{\alpha}}\rangle}{\epsilon-\epsilon_{\bar{\alpha}}} + \frac{\langle f_\alpha^+ f_{\bar{\alpha}}\rangle}{\epsilon-\epsilon_{\bar{\alpha}}-U}$ means off-diagonal elements of the retarded Green's function of two coupled dots without the connection to the leads. The elements of the retarded self-energy, $\begin{pmatrix}\bar{\Sigma}_{++}^r(\epsilon) & \bar{\Sigma}_{+-}^r(\epsilon)\\ \bar{\Sigma}_{-+}^r(\epsilon) & \bar{\Sigma}_{--}^r(\epsilon)\end{pmatrix} = \begin{pmatrix}\bar{\Sigma}_{++,L}^r(\epsilon) & \bar{\Sigma}_{+-,L}^r(\epsilon)\\ \bar{\Sigma}_{-+,L}^r(\epsilon) & \bar{\Sigma}_{--,L}^r(\epsilon)\end{pmatrix} + \begin{pmatrix}\bar{\Sigma}_{++,R}^r(\epsilon) & \bar{\Sigma}_{+-,R}^r(\epsilon)\\ \bar{\Sigma}_{-+,R}^r(\epsilon) & \bar{\Sigma}_{--,R}^r(\epsilon)\end{pmatrix}$, due to

the coupling between the quantum dot system and the two leads, are given by

$$\bar{\Sigma}^r_{\alpha\alpha,\nu}(\epsilon) = -\mathrm{i}\frac{\Gamma}{2} + \mathrm{i}\delta_\alpha \frac{\Gamma}{2}\cos(\eta_\nu\phi/2 - \theta)\sin 2\beta, \tag{27}$$

$$\bar{\Sigma}^r_{\alpha\tilde{\alpha},\nu}(\epsilon) = \mathrm{i}\frac{\Gamma}{2}(\sin^2\beta \mathrm{e}^{-\mathrm{i}\gamma_{\alpha\tilde{\alpha}}\eta_\nu\phi/2} - \cos^2\beta \mathrm{e}^{\mathrm{i}\gamma_{\alpha\tilde{\alpha}}\eta_\nu\phi/2}\mathrm{e}^{-2\mathrm{i}\gamma_{\alpha\tilde{\alpha}}\theta}), \tag{28}$$

$$(\delta_+ = 1, \delta_- = -1;\ \gamma_{+-} = 1, \gamma_{-+} = -1;\ \nu = L, R;\ \eta_L = 1, \eta_R = -1).$$

$\bar{\Sigma}^r_{\alpha\alpha(\tilde{\alpha}),\nu}(\epsilon)$ is independent of energy under the wide-band limit approximation. We assumed that the DQDs are attached to the left and right leads with equal strengths in the absence of the magnetic flux. Therefore, the elements of the tunnelling matrix are identical, $\Gamma^\nu_j = \Gamma$ ($j = 1, 2$; $\nu = L, R$). Using equations (25)–(28), we obtain the elements of the retarded Green's function

$$G^r_{++}(\epsilon) = \{g^r_{++}(\epsilon) + [g^r_{+-}(\epsilon)g^r_{-+}(\epsilon) - g^r_{++}(\epsilon)g^r_{--}(\epsilon)]\overline{\Sigma}^r_{--}\}/D, \tag{29}$$

$$G^r_{+-}(\epsilon) = -\{g^r_{+-}(\epsilon) + [g^r_{+-}(\epsilon)g^r_{-+}(\epsilon) - g^r_{++}(\epsilon)g^r_{--}(\epsilon)]\overline{\Sigma}^r_{+-}\}/D, \tag{30}$$

$$G^r_{-+}(\epsilon) = -\{g^r_{-+}(\epsilon) + [g^r_{+-}(\epsilon)g^r_{-+}(\epsilon) - g^r_{++}(\epsilon)g^r_{--}(\epsilon)]\overline{\Sigma}^r_{-+}\}/D, \tag{31}$$

$$G^r_{--}(\epsilon) = \{g^r_{--}(\epsilon) + [g^r_{+-}(\epsilon)g^r_{-+}(\epsilon) - g^r_{++}(\epsilon)g^r_{--}(\epsilon)]\overline{\Sigma}^r_{++}\}/D, \tag{32}$$

where

$$D = [1 - g^r_{++}\overline{\Sigma}^r_{++} + g^r_{+-}\overline{\Sigma}^r_{-+}][1 - g^r_{--}\overline{\Sigma}^r_{--} + g^r_{-+}\overline{\Sigma}^r_{+-}] - [g^r_{++}\overline{\Sigma}^r_{+-} - g^r_{+-}\overline{\Sigma}^r_{--}][g^r_{--}\overline{\Sigma}^r_{-+} - g^r_{-+}\overline{\Sigma}^r_{++}]. \tag{33}$$

Note that the electron occupation of the molecular states $\langle f^\dagger_+ f_+\rangle$, $\langle f^\dagger_- f_-\rangle$ and the correlation value $\langle f^\dagger_+ f_-\rangle$, $\langle f^\dagger_- f_+\rangle$ must be calculated self-consistently

$$\langle f^\dagger_\alpha f_\alpha\rangle = -\mathrm{i}\int \frac{\mathrm{d}\epsilon}{2\pi}\mathbf{G}^<_{\alpha\alpha}(\epsilon), \tag{34}$$

$$\langle f^\dagger_\alpha f_{\tilde{\alpha}}\rangle = -\mathrm{i}\int \frac{\mathrm{d}\epsilon}{2\pi}\mathbf{G}^<_{\tilde{\alpha}\alpha}(\epsilon). \tag{35}$$

In the molecular state representation, the Green's function $\mathbf{G}^{r,<}(\epsilon)$ is expressed by 2×2 matrices $\mathbf{G}^{r,<}(\epsilon) = \begin{pmatrix} G^{r,<}_{++}(\epsilon) & G^{r,<}_{+-}(\epsilon) \\ G^{r,<}_{-+}(\epsilon) & G^{r,<}_{--}(\epsilon)\end{pmatrix}$. The lesser Green's function $\mathbf{G}^<(\epsilon)$ can be calculated by the formula

$$\mathbf{G}^<(\epsilon) = \mathbf{G}^r(\epsilon)\bar{\Sigma}^<(\epsilon)\mathbf{G}^a(\epsilon), \tag{36}$$

where the lesser self-energy $\bar{\sum}^<(\epsilon)$ is obtained by

$$\bar{\Sigma}^<(\epsilon) = -f_L(\epsilon)(\bar{\Sigma}^r_L - \bar{\Sigma}^a_L) - f_R(\epsilon)(\bar{\Sigma}^r_R - \bar{\Sigma}^a_R), \tag{37}$$

with the Fermi–Dirac distribution $f_\nu(\epsilon) = 1/[1+\mathrm{e}^{(\epsilon-\mu_\nu)/k_\mathrm{B}T}]$ ($\nu = L, R$) for lead ν. From the relationships of $\mathbf{G}^a(\epsilon) = [\mathbf{G}^r(\epsilon)]^\dagger$ and $\Sigma^a_\nu(\epsilon) = [\Sigma^r_\nu(\epsilon)]^\dagger$ ($\nu = L, R$), the advanced Green's function and self-energies can be obtained. The DOS in state α is calculated in terms of the diagonal elements of the retarded Green's function $\mathbf{G}^r$

$$\rho_\alpha = -\frac{1}{\pi}\,\mathrm{Im}\,G^r_{\alpha\alpha}, \qquad (\alpha = +, -). \tag{38}$$

4. Tunnelling current formula

Now let us study transport properties of the quantum device by using the Keldysh Green's function in the new basis of equations (7) and (8). According to the work of Jauho *et al* [33], the current from the left (right) lead to the double quantum dots can be expressed as

$$I_{L(R)} = \frac{\mathrm{i}e}{\hbar}\int \frac{\mathrm{d}\epsilon}{2\pi}\,\mathrm{Tr}\{\bar{\Gamma}^{L(R)}[\mathbf{G}^<(\epsilon) + f_{L(R)}(\epsilon)(\mathbf{G}^r(\epsilon) - \mathbf{G}^a(\epsilon))]\}. \tag{39}$$

The linewidth matrix function of lead $\bar{\Gamma}^{\nu}$ describes the tunnelling coupling of the two dots to lead ν

$$\bar{\Gamma}^{L} = \Gamma \begin{pmatrix} 1 - \sin 2\beta \cos(\phi/2 - \theta) & \cos^2 \beta e^{i(\phi/2-2\theta)} - \sin^2 \beta e^{-i\phi/2} \\ \cos^2 \beta e^{-i(\phi/2-2\theta)} - \sin^2 \beta e^{i\phi/2} & 1 + \sin 2\beta \cos(\phi/2 - \theta) \end{pmatrix} \tag{40}$$

$$\bar{\Gamma}^{R} = \Gamma \begin{pmatrix} 1 - \sin 2\beta \cos(\phi/2 + \theta) & \cos^2 \beta e^{-i(\phi/2+2\theta)} - \sin^2 \beta e^{i\phi/2} \\ \cos^2 \beta e^{i(\phi/2+2\theta)} - \sin^2 \beta e^{-i\phi/2} & 1 + \sin 2\beta \cos(\phi/2 + \theta) \end{pmatrix}. \tag{41}$$

It is noticed that the off-diagonal matrix elements of $\bar{\Gamma}^{\nu}$ are complex numbers in the presence of the AB phase. In the steady state, the current is uniform, so that $I = I_L = -I_R$; the total current I can be written as $I = (I_L - I_R)/2$. Using equation (39), the general expression of the dc current can be expressed as

$$I = \frac{ie}{2\hbar} \int \frac{d\epsilon}{2\pi} \mathrm{Tr}\{[\bar{\Gamma}^{L} - \bar{\Gamma}^{R}]\mathbf{G}^{<}(\epsilon) + [\bar{\Gamma}^{L} f_L(\epsilon) - \bar{\Gamma}^{R} f_R(\epsilon)][\mathbf{G}^{r}(\epsilon) - \mathbf{G}^{a}(\epsilon)]\}. \tag{42}$$

5. Numerical results and discussion

In this section, we discuss two cases: the covalent bonding limit ($\epsilon_1 = \epsilon_2 = 2\Gamma$) and the general case with a nonzero difference in the levels of the two dots $\Delta\epsilon = \epsilon_1 - \epsilon_2$. When the interdot coulomb interaction is ignored, the system can be modelled by a non-interacting two-site Anderson Hamiltonian. Such a system has been studied extensively in the literature [5–10, 12]. It is well known that the width of the Fano resonance in the linear conductance spectrum is zero in the absence of the magnetic field when the system is perfectly symmetrical. The reason is that the antibonding states are decoupled from the leads due to the destructive quantum interference between two different pathways across the quantum dot molecule [6]. When the external magnetic field is switched on, or when the energy levels of the two different quantum dots are not equal, the Fano resonance will occur even for the perfectly symmetrical system. In the present work, we concentrate on the effects of the interdot Coulomb interaction U and the inhomogeneous magnetic flux θ. The interdot coulomb interaction may give rise to the Kondo effect when the temperature is low enough [32].

5.1. $\Delta\epsilon = 0$

We first study the symmetrical system in the covalent limit ($\Delta\epsilon = \epsilon_1 - \epsilon_2 = 0$). The parameters for our calculations are taken as $\epsilon_1 = \epsilon_2 = \epsilon_0 = 2\Gamma$, $U = 5\Gamma$, and $t_c = \Gamma$. For this case, the broadenings of the two molecular states $\overline{\Gamma}_{++}$ and $\overline{\Gamma}_{--}$ can be calculated by the retarded self-energy due to the coupling to the leads,

$$\overline{\Gamma}_{++} = i2\overline{\Sigma}^{r}_{++} = 2\Gamma \left(1 - \cos\frac{\phi}{2}\cos\theta\right) \tag{43}$$

and

$$\overline{\Gamma}_{--} = i2\overline{\Sigma}^{r}_{--} = 2\Gamma \left(1 + \cos\frac{\phi}{2}\cos\theta\right). \tag{44}$$

The widths of the two states have the period of 4π for AB phase ϕ and 2π for the magnetic flux imbalance of θ, which provides the possibility to control the quantum transport through the parameters ϕ and θ. Most importantly, the antibonding state will be decoupled from the leads when $\cos\frac{\phi}{2}\cos\theta \to 1$, and the bonding state is decoupled from the leads when $\cos\frac{\phi}{2}\cos\theta \to -1$. The disappearance of the antibonding state is the consequence of the destructive quantum interference between different pathways in the absence of the magnetic flux in a symmetrical parallel geometry [6].

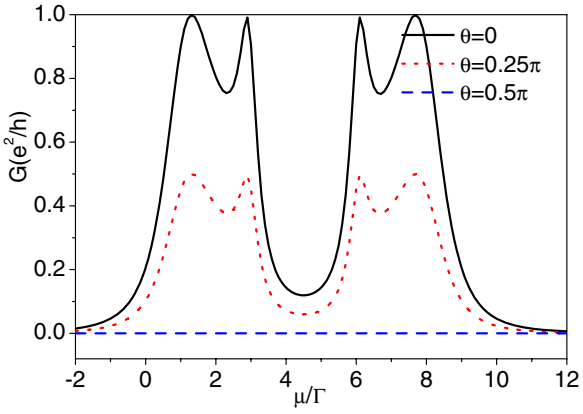

Figure 2. The linear differential conductance G as a function of the chemical potential μ with a fixed total AB phase $\phi = (2n + 1)\pi$ for several flux imbalances. The solid, dotted, and dashed lines correspond to the cases of $\theta = 0, 0.25\pi$, and 0.5π, respectively. Other parameters are given by $t_c = \Gamma$, $\epsilon_1 = \epsilon_2 = 2\Gamma$, $U = 5\Gamma$, and $k_B T = 0.02\Gamma$.

The couplings between the two molecular states and the leads will be equal, $\overline{\Gamma}_{++} = \overline{\Gamma}_{--} = \Gamma$, when $\phi = (2n+1)\pi$ or $\theta = (2n+1)\pi/2$, $(n = 0, 1, 2, \ldots)$. Using the generalized Landauer formula at finite temperature, the current through the double quantum dots is related to the transmission coefficient $T(\epsilon)$ [11]

$$I = \frac{e}{h}\int \mathrm{d}\epsilon\,[f_L - f_R]T(\epsilon) = \frac{e}{h}\int \mathrm{d}\epsilon[f_L - f_R]\,\mathrm{Tr}[\bar{\Gamma}^L \mathbf{G}^a \bar{\Gamma}^R \mathbf{G}^r]. \tag{45}$$

When the source–drain voltage is small, the quantum system is in the linear response regime. The linear conductance G is given

$$G = \frac{e^2}{h}\int \mathrm{d}\epsilon\; f_L'(\epsilon)T(\epsilon) \tag{46}$$

where $f_L'(\epsilon)$ is the derivative of the Fermi–Dirac distribution function in the left lead. At the lower temperature, $f_L'(\epsilon)$ can approximate a δ function.

The linear conductance G, including strong interdot interaction, is illustrated in figure 2 as a function of the chemical potential $\mu_L = \mu_R = \mu$ for several different values of inhomogeneous magnetic flux θ with a fixed magnetic flux $\phi = (2n+1)\pi$ at finite temperature ($k_B T = 0.02\Gamma$). Four apparent resonant conductance peaks related to four electronic states with energies ϵ_-, ϵ_+, $\epsilon_- + U$ and $\epsilon_+ + U$ are observed due to the interdot interaction U and the quantum coupling between the two quantum dots. Two wide conductance peaks are located in the vicinity of ϵ_- and $\epsilon_+ + U$, and two narrow conductance peaks appear in the vicinity of ϵ_+ and $\epsilon_- + U$, in comparison to the case without the interdot coulomb interaction $U = 0$ where only a single peak occurs [10]. This indicates that the interdot Coulomb interaction plays an important role in our system, and the widths of the conductance peaks are modified by the electron numbers on states '+' and '−'. In fact, the state with energy $\epsilon_-(\epsilon_+)$ is weighted by the possibility $1 - n_+(1 - n_-)$, and the state with energy $\epsilon_+ + U(\epsilon_- + U)$ is weighted by the possibility $n_-(n_+)$. For $\theta = 0$, the heights of the four conductance peaks approach e^2/h, which implies that four ideal channels may be developed. The heights of the conductance peaks become lower with the broader full width at half maximum, when θ increases from 0 to $\pi/2$. Moreover, all conductance peaks disappear when $\theta = \pi/2$, and all electron states become localized in the dot molecule, so that they do not contribute to any electron transmission through the double dots.

Figure 3 shows the linear conductance G versus the chemical potential μ for the fixed inhomogeneous magnetic flux $\theta = (2n + 1)\pi/2$ and different values of AB phase ϕ. For the case of $U = 0$, two conductance peaks around Γ and 3Γ approach e^2/h for $\phi = 0$. As

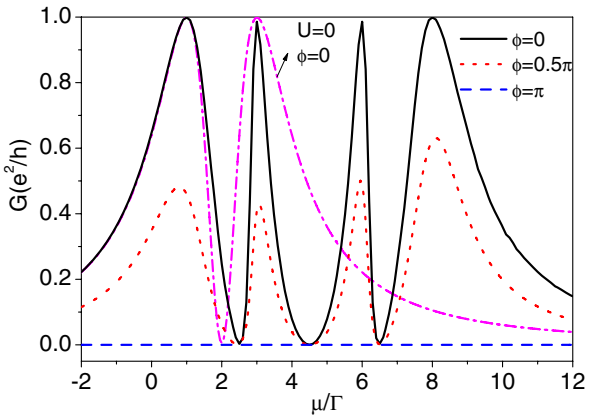

Figure 3. The linear differential conductance G as a function of the chemical potential μ with a fixed flux imbalance $\theta = (2n + 1)\pi/2$ for several total AB phases. The solid, dotted, and dashed curves correspond to the cases of $\phi = 0, 0.5\pi$, and π, respectively. The dash–dotted line corresponds to the case of $U = 0$ and $\phi = 0$. Other parameters are chosen as the ones in figure 2.

a result of the destructive interference, an antiresonance dip is observed with the chemical potential equal to 2Γ. When strong interdot coulomb interaction $U \gg \Gamma$ and $U \gg t_c$ is considered, the antiresonance point moves the right way, and the other antiresonance point appears at the same energies displaced by U. The second peak becomes narrower, and the other pair of peaks appears around the energies $\epsilon_- + U$ and $\epsilon_+ + U$ due to the interdot coulomb interaction. The antiresonance phenomenon has been widely studied based on the single-particle Green's function using the noninteracting two-site Anderson model in the previous theoretical work [5–10]. On increasing ϕ from 0 to π, the widths and heights of conductance become narrower and lower, respectively. The positions of these antiresonances are fixed for the AB phase. When the AB phase is equal to π, the conductance disappears completely, and the two-dot device becomes an electrical insulator.

Fano effects have been investigated widely in mesoscopic transport without considering the interdot interaction [5–10, 34], since its first observation in the regime of atomic physics due to the interference between the localized state and the continuum states [35]. Two quantum dots can be coupled to form an artificial molecule, which offers a good opportunity to study the quantum interference when the molecule is attached in parallel configuration to two external electron reservoirs. As reported by Orellana *et al* [7], the linear conductance spectrum is composed of a Breit–Wigner resonance located around the electron state with a wide DOS (density of states) peak and a Fano resonance located around the other electron state with a narrow DOS peak. In the present work, we are mainly interested in the case in the presence of the interdot interaction U and the magnetic flux imbalance θ with the fixed total magnetic flux, for example $\phi = 0.2\pi$. The linear conductance G and DOS $\rho_\alpha(\alpha = +, -)$ as a function of the chemical potential μ at finite temperature $k_B T = 0.02\Gamma$ for four different values of θ are plotted in the left and right columns in figure 4. From the DOS curve, we find the DOSs of four possible electronic states have different widths due to interdot interaction. Two Breit–Wigner resonances centred around the strongly coupled electronic states with broad DOS peaks and two Fano resonances centred at the weakly coupled electronic states with narrow DOS peaks are observed in the linear conductance curve. This is due to the fact that the phase shift of π happens when the chemical potential μ sweeps across the weakly coupled electronic states, whereas the invariance in the phase for the strongly coupled electron states is very small. Thus,

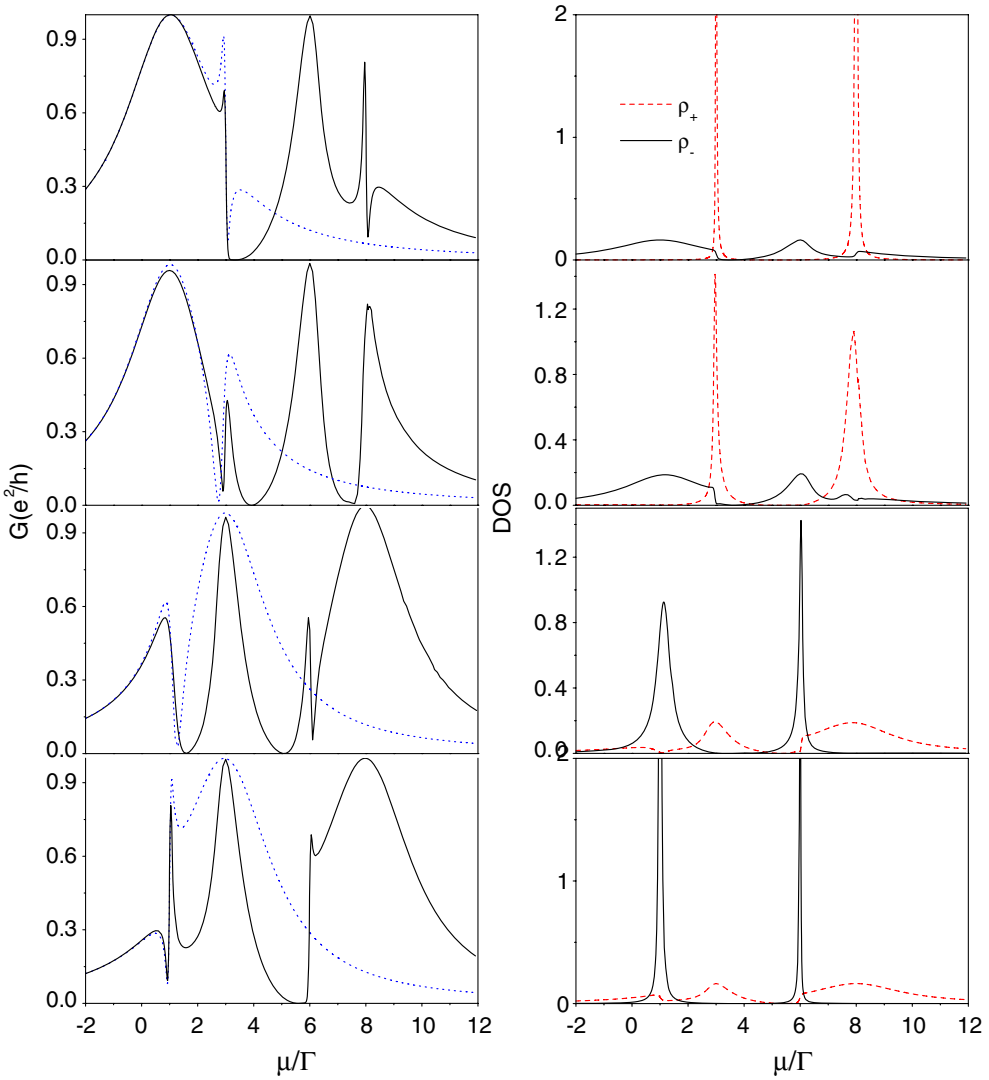

Figure 4. The linear differential conductance G and LDOS ρ_α ($\alpha = +, -$) as a function of the chemical potential μ for several flux imbalances: 0, $\pi/4$, $3\pi/4$ and π from top to bottom. All dash–dotted lines show the case of $U = 0$. Other parameters are chosen as the ones in figure 2.

Fano effects occur at the weakly coupled electron states as a result of quantum interference. For $\theta = 0$, there are two wide DOS peaks centred in the vicinity of ϵ_- and $\epsilon_- + U$ and two narrow DOS peaks centred in the vicinity of ϵ_+ and $\epsilon_+ + U$, which results in two Breit–Wigner and two Fano resonances in the linear conductance spectrum. The dotted lines shows the case of $U = 0$. From our numerical results, we see that the line shape of conductance peaks around ϵ_- and ϵ_+ may be modified by interdot interaction, and the other group conductance peaks consisting of Breit–Wigner and Fano resonances appear as shown in figure 4. The line shape of the linear conductance $G(\theta)$ centred at $\epsilon_+(\epsilon_-)$ is changed into that of the linear conductance $G(\pi - \theta)$ centred at $\epsilon_- + U(\epsilon_+ + U)$. We note that the heights of two Fano peaks with $\theta = 0$ or $\theta = \pi$ are less than e^2/h, while the heights of the Breit–Wigner peaks always approach e^2/h at the

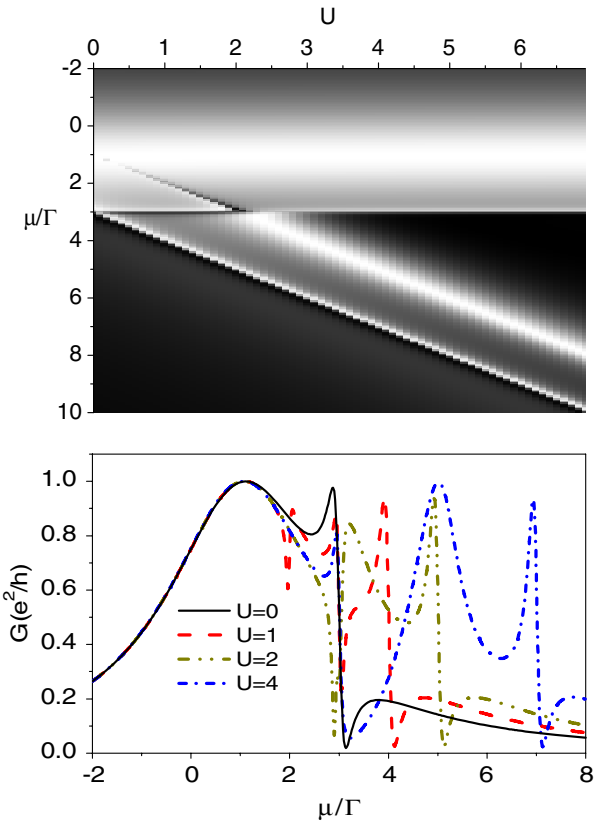

Figure 5. The linear differential conductance G as a function of the chemical potential μ and the interdot interaction U is plotted on the upper panel. The linear differential conductance as a function of the chemical potential μ under several different values of U. Other parameters are chosen as $\epsilon_1 = \epsilon_2 = 2\Gamma$, $\phi = 0.3\pi$, and $t_0 = \Gamma$.

above temperature. The reason is that the Breit–Wigner peaks correspond to strongly coupled electric states, and Fano peaks originate from the weakly coupled electric states.

In figure 5, we plot the dependence of the linear conductance on the interdot interaction U. G versus the chemical potential μ and the interdot interaction is plotted in the upper panel. The parameters of the system are chosen as $\phi = 0.3\pi$, $\epsilon_1 = \epsilon_2 = \epsilon_0 = 2\Gamma$, and $t_0 = \Gamma$. As in the above discussion, four electronic states appear in the quantum system in the presence of the interdot interaction, at $\epsilon_0 - t_0$, $\epsilon_0 + t_0$, $\epsilon_0 - t_0 + U$, and $\epsilon_0 + t_0 + U$, respectively. The bright region represents the high linear conductance, and the dark region is the low linear conductance. Fano effects often happen in the conterminous region between the bright region and dark region. For example, Fano peaks exist in the vicinity of lines $\mu = \epsilon_0 + t_0$ and $\mu = \epsilon_0 + t_0 + U$. We note that Fano effects also occur in the vicinity of the line $\mu = \epsilon_0 - t_0 + U$ when $0 < U < 2\Gamma$. The Breit–Wigner peak induced by state $\epsilon_0 - t_0$ distributes the bright region near the line $\mu = \epsilon_0 - t_0$. We plot the linear conductance as a function of the chemical potential μ at different values of U in the lower panel of figure 5. In particular, states $\epsilon_0 + t_0$ and $\epsilon_0 - t_0 + U$ are superposed when $U = 2\Gamma$. The conductance spectrum consists of the Breit–Wigner resonance centred at $\epsilon_0 - t_0$ and two Fano resonances centred at $\epsilon_0 + t_0$ and $\epsilon_0 + t_0 + U$. When $0 < U < 2\Gamma$, another Fano resonance occurs at $\epsilon_0 - t_0 + U$. For the strong interdot interaction ($U = 4\Gamma$), the conductance spectrum consists of two Breit–Wigner resonances and two Fano resonances as in the discussion in figure 4.

We pay some attention to the case in the absence of the interdot tunnelling coupling $t_c = 0$ for several values of total magnetic flux ϕ. Figure 6 shows the dependence of the

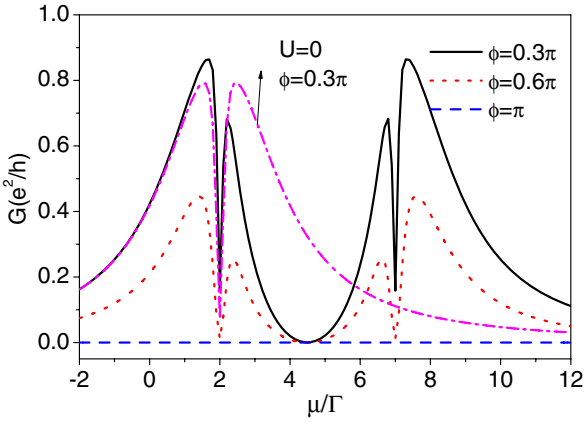

Figure 6. The linear differential conductance G as a function of the chemical potential μ in the absence of interdot tunnelling coupling for several AB phases. The solid, dotted, and dashed lines correspond to the cases of $\phi = 0.3\pi, 0.6\pi$, and π, respectively. The dash–dotted line shows the case with $U = 0$ and $\phi = 0.3\pi$. Other parameters are chosen as the ones in figure 2.

linear conductance on the chemical potential μ. The temperature is $k_B T = 0.02\Gamma$. The same energy levels of the double quantum dots and interdot interaction are set to be 2Γ and 5Γ, respectively. We note that two dips of the linear conductance appear at $\epsilon = \epsilon_0$ and $\epsilon = \epsilon_0 + U$ when a magnetic field ϕ is applied through the set-up due to quantum interference. As ϕ increases, the two dips approach zero, and the heights and widths of the conductance peaks are lower and narrower, respectively. The amplitudes of the middle two peaks are less than those of the outside two peaks. The dash–dotted line shows the case of $U = 0$ and $\phi = 0.3\pi$. Two conductance peaks with the same heights appear at the chemical potentials 1Γ and 3Γ, respectively. When strong interdot interaction is considered, the heights of the two peaks are modified by U. The results come from the fact that flip processes between $+$ and $-$ are considered as shown at equation (23).

Little attention has been paid to the non-equilibrium situation expect for a very recent work [12]. Experimentally, the bias V is applied across two electrodes, which leads to the potential $\mu_L = E_F + V/2$ in the left electrode and $\mu_R = E_F - V/2$ for the right electrode. Here we take $E_F = 0$. The tunnelling current through the quantum device can be calculated by equation (45), and the differential conductance is obtained by using the relation $G_V = dI/dV$. In figure 7, we plot the current I on the lower panel and the corresponding differential conductance G_V on the upper panel as functions of the applied voltage. The interdot interaction is $U = 5\Gamma$ and the temperature is $k_B T = 0.02\Gamma$. Related to the smooth increasing of tunnelling current, the positive differential conductance (PDC) peaks often occur when the Fermi levels of the two leads sweep across the strongly coupled electronic states, whereas the negative differential conductance (NDC) dips, related to the abrupt reduction of the tunnelling current, occur when the chemical potentials in the leads sweep cross the weakly coupled electronic states. For $\theta = 0$, two NDC dips are observed in the vicinity of ϵ_+ and $\epsilon_+ + U$. The PDC peaks are centred around ϵ_- and $\epsilon_- + U$. When $\theta = \pi/2$, the NDC phenomenon almost disappears and eight conductance peaks appear due to $\overline{\Gamma}_{--} = \overline{\Gamma}_{++}$. When θ is further increased to π, the NDC dips re-appear. However, in this case, one NDC dip occurs around ϵ_- and the other NDC dip emerges near $\epsilon_- + U$. In order to probe the origin of the NDC, we plot the difference of the electron numbers in two dots, $\Delta N(V) = N_1(V) - N_2(V)$, as a function of V in figure 8. $N_j(V)$ is the occupation number in dot j when bias V is applied across the quantum device,

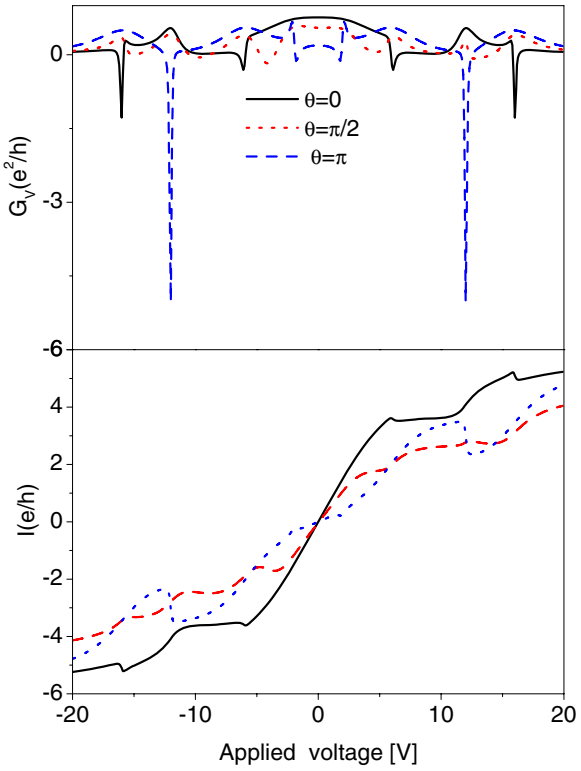

Figure 7. Differential conductance G_V and tunnelling current I as a function of bias V with a fixed total AB phase $\phi = 0.3\pi$ for several different values of flux imbalance. The solid, dotted, and dashed curves show the cases for $\theta = 0, 0.5\pi$, and π, respectively. Other parameters are chosen as the ones in figure 2. The temperature parameter is taken as $k_B T = 0.02\Gamma$.

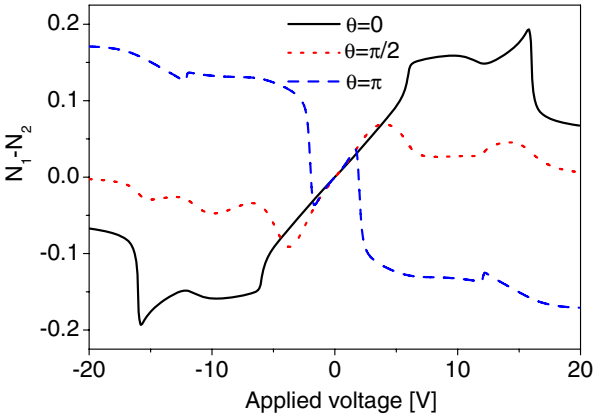

Figure 8. The difference $(N_1 - N_2)$ of electron occupation number between two dots as a function of the bias V for various flux imbalances. Other parameters are chosen as in figure 6.

which is calculated by the relationships

$$N_1 = \tfrac{1}{2}(\langle n_+\rangle + \mathrm{e}^{-\mathrm{i}\theta}\langle f_+^+ f_-\rangle + \mathrm{e}^{\mathrm{i}\theta}\langle f_-^+ f_+\rangle + \langle n_-\rangle) \tag{47}$$

and

$$N_2 = \tfrac{1}{2}(\langle n_+\rangle - \mathrm{e}^{-\mathrm{i}\theta}\langle f_+^+ f_-\rangle - \mathrm{e}^{\mathrm{i}\theta}\langle f_-^+ f_+\rangle + \langle n_-\rangle). \tag{48}$$

It is found that the NDC occurs when ΔN changes drastically, as shown in figure 8. For example, ΔN has a abrupt change when the chemical potentials sweep cross the weakly coupled electronic states ϵ_+ and $\epsilon_+ + U$ for $\theta = 0$. The abrupt change in ΔN happens around ϵ_- and $\epsilon_- + U$ for $\theta = \pi$. When $\theta = \pi/2$, ΔN, as a function of V, exhibits a smooth change

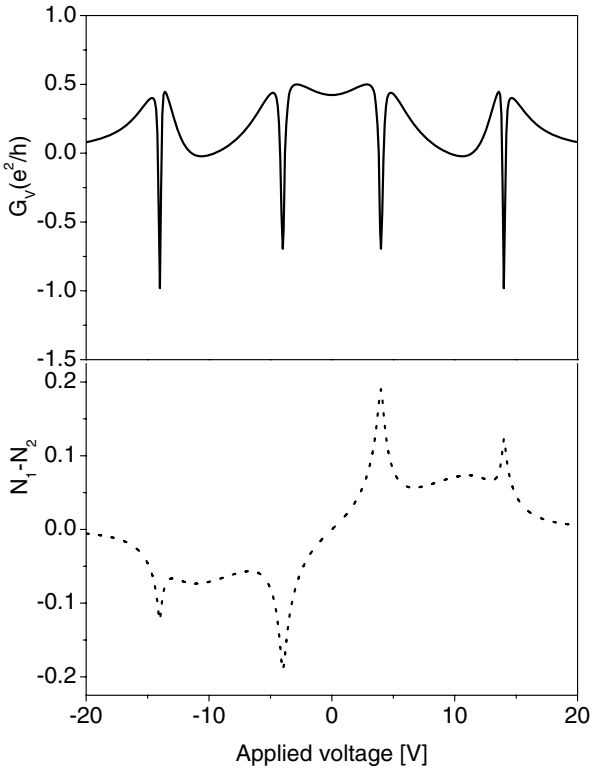

Figure 9. Differential conductance G_{V} and the difference $(N_1 - N_2)$ of electron occupation number between two dots as a function of the bias V for the case of $t_{\mathrm{c}} = 0$. Other parameters are chosen as in figure 6.

when the Fermi levels move across the four states. Figure 9 presents the non-equilibrium case in the absence of interdot coupling $t_{\mathrm{c}} = 0$ with a fixed total magnetic flux $\phi = 0.3\pi$. Four NDC dips happen when the Fermi levels are aligned with ϵ_0 and $\epsilon_0 + U$ due to the interdot interaction and quantum inference, and abrupt changes in ΔN are observed around the above four points.

5.2. $\Delta\epsilon \neq 0$

In this section, the detuning $\Delta\epsilon$ of electronic levels in the two quantum dots will be studied. The bare levels in the two dots are fixed at $\epsilon_1 = \epsilon_0 + \Delta\epsilon/2$ and $\epsilon_2 = \epsilon_0 - \Delta\epsilon/2$, respectively. Here the parameter ϵ_0 is taken to be 2Γ. For the sake of simplicity, we still assume $\Gamma_{i,j} = t_{\mathrm{c}} = \Gamma$ and $\varphi = \theta = 0$. No magnetic flux threads through the device. The broadenings of the two molecular states $\overline{\Gamma}_{++}$ and $\overline{\Gamma}_{--}$ can be written as, respectively

$$\overline{\Gamma}_{++} = \mathrm{i}2\overline{\Sigma}^{r}_{++} = 2\Gamma(1 - \sin 2\beta) \tag{49}$$

and

$$\overline{\Gamma}_{--} = \mathrm{i}2\overline{\Sigma}^{r}_{--} = 2\Gamma(1 + \sin 2\beta). \tag{50}$$

The widths of the two molecular states are sensitive to parameter β. β is adjusted by $\Delta\epsilon$ and the interdot coupling t_{c}. The linear conductance G, DOS ρ_+ (soild line), and ρ_- (dotted line) as functions of the chemical potential μ are plotted in the left column and right column in figure 10 for different values of detuning $\Delta\epsilon$. For $\Delta\epsilon = \Gamma$, ρ_+ displays two narrow peaks centred at ϵ_+ and $\epsilon_+ + U$ with different heights and widths as shown in figure 10. ρ_- shows two wide peaks centred at ϵ_- and $\epsilon_- + U$. When the chemical potential μ sweeps wide peaks, Breit–Wigner

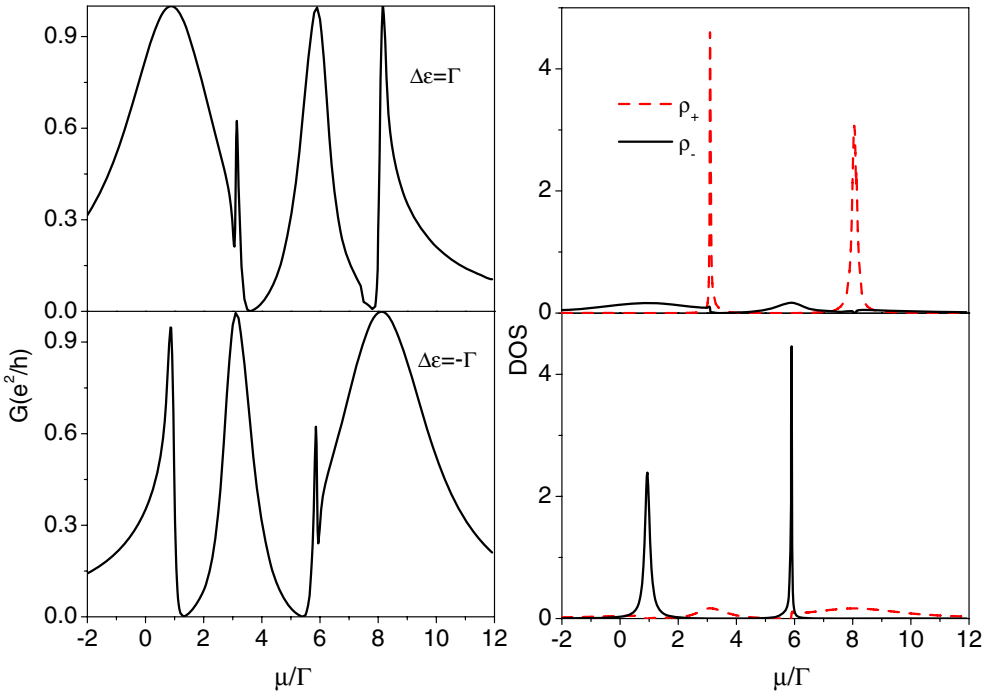

Figure 10. Differential conductance G and the LDOS ρ_+ and ρ_- as the chemical potential μ for $\Delta\epsilon = \Gamma$ and $\Delta\epsilon = -\Gamma$. Other parameters are chosen as in figure 2.

resonances occur due to $\bar{\Gamma}_{++} \gg \bar{\Gamma}_{--}$. At the same time, two Fano resonances occur when μ sweeps two narrow peaks. When $\Delta\epsilon = -\Gamma$, two Breit–Wigner resonances evolve into two Fano resonances and two Fano resonances evolve into two Breit–Wigner resonances due to $\bar{\Gamma}_{++} \ll \bar{\Gamma}_{--}$.

It is worthwhile to mention that the differential conductance and DOS are expected to have no significant change in the asymmetrical case ($\Gamma^L \neq \Gamma^R$), which have thus been neglected.

6. Summary

By using the Keldysh Green's function method, we have studied the electronic transport properties of the coupled double dot connected in symmetrically parallel configuration to the leads with the interdot Coulomb interaction. Four electron states are formed in the presence of strong interdot Coulomb interaction, which leads to four peaks in both the conductance and DOS spectra. As a result of quantum interference effects of the electron transition through weakly coupled and strongly coupled electronic states, the linear conductance spectrum is often composed of two Breit–Wigner resonances and two Fano resonances when the magnetic field is switched on or when there exists a finite difference between the energies of the different quantum dots in the symmetrical coupling between the quantum set-up and the leads. It has been found that the negative differential conductance (NDC) corresponding to the abrupt change in the difference of the electron occupation number in the different quantum dots may happen when the Fermi levels in the leads are moved across the weakly coupled energy levels by the external bias. The parallel-coupled DQD system may be used as a promising candidate for a quantum qubit in quantum computation in the future. Quantum computing may benefit from

the study of the Aharonov–Bohm ring with two quantum dots as a promising phase-controlled device.

Acknowledgments

The authors thank the National Natural Science Foundation of China for support under grant Nos 10574024 and 90606024, and the Fudan High-End Computing Centre.

References

[1] Gores J, Goldhaber-Gordon D, Heemeyer S, Kastner M A, Shtrikman H, Mahalu D and Meirav U 2000 *Phys. Rev.* B **62** 2188
[2] Liang W, Bockrath M and Park H 2002 *Phys. Rev. Lett.* **88** 126801
[3] For a review see for example Vanderwiel W G, Franceschi S D, Elgerman J M, Tarucha S and Kouwenhoven L P 2003 *Rev. Mod. Phys.* **75** 1
[4] Liu Y S, Chen H, Fan X H and Yang X F 2006 *Phys. Rev.* B **73** 115310
[5] Kubala B and König J 2002 *Phys. Rev.* B **65** 245301
[6] Ladrón de Guevara M L, Claro F and Orellana P A 2003 *Phys. Rev.* B **67** 195335
[7] Orellana P A, Ladrón de Guevara M L and Claro F 2004 *Phys. Rev.* B **70** 233315
[8] Bai Z M, Yang M F and Chen Y C 2004 *J. Phys.: Condens. Matter* **16** 2053
[9] Kang K and Cho S Y 2004 *J. Phys.: Condens. Matter* **16** 117
[10] Lu H Z, Lü R and Zhu B F 2005 *Phys. Rev.* B **71** 235320
[11] Wu B H and Cao J C 2004 *J. Phys.: Condens. Matter* **16** 8285
[12] Chi F and Li S S 2005 *J. Appl. Phys.* **97** 123704
[13] Cho S Y, McKenzie R H, Kang K C and Kim C K 2003 *J. Phys.: Condens. Matter* **15** 1147
[14] Cho S Y and McKenzie R H 2005 *Phys. Rev.* B **71** 045317
[15] Kubo T, Tokura Y, Hatano T and Tarucha S 2006 *Preprint* cond-mat/0602539 (unpublished)
[16] Holleitner A W, Decker C R, Qin H, Eberl K and Blick R H 2001 *Phys. Rev. Lett.* **87** 256802
Holleitner A W, Blick R H, Hüttel A K, Eberl K and Kotthaus J P 2002 *Science* **297** 70
Holleitner A W, Blick R H and Eberl K 2003 *Appl. Phys. Lett.* **82** 1887
[17] Kobayashi K, Aikawa H, Katsumoto S and Iye Y 2002 *Phys. Rev. Lett.* **88** 256806
[18] Bulka B R and Kostyrko T 2004 *Phys. Rev.* B **70** 205333
[19] Meden V and Marquardt F 2006 *Phys. Rev. Lett.* **96** 146801
[20] Kuo D M T and Li P W 2006 *Japan. J. Appl. Phys.* 1 **45** 2881
[21] Lu H Z, Lü R and Zhu B F 2006 *J. Phys.: Condens. Matter* **18** 8961
[22] Loss D and Sukhorukov E V 2000 *Phys. Rev. Lett.* **84** 1035
[23] Bayer M, Hawrylak P, Hinzer K, Fafard S, Korkusinski M, Wasilewski Z R, Stern O and Forchel A 2001 *Science* **291** 7451
[24] Fujisawa T, Hayashi T and Hirayama Y 2004 *J. Vac. Sci. Technol.* B **22** 2053
[25] Hayashi T, Fujisawa T, Cheong H D, Jeong Y H and Hirayama Y 2003 *Phys. Rev. Lett.* **91** 226804
[26] Stafford C A and Wingreen N S 1996 *Phys. Rev. Lett.* **76** 1916
[27] Mourokh L G and Smirnov A Y 2005 *Phys. Rev.* B **72** 033310
[28] Sun Q F and Guo H 2002 *Phys. Rev.* B **66** 155308
[29] Bruus H and Flenserg K 2004 Many-Body Quantum Theory *in Condensed Matter Physics: An Introduction* (Oxford: Oxford University Press)
[30] Haug H and Jauho A P 1996 *Quantum Kinetics in Transport and Optics of Semiconductors* (Berlin: Springer)
[31] Rudziński W, Barnaś J, Świrkowicz R and Wilczyński M 2005 *Phys. Rev.* B **71** 205307
[32] Kashcheyevs V, Schiller A, Aharony A and Entin-Wohlman O 2007 *Phys. Rev.* B **75** 115313
[33] Jauho A P, Wingreen N S and Meir Y 1994 *Phys. Rev.* B **50** 5528
[34] Shahbazyan T V and Raikh M E 1994 *Phys. Rev.* B **49** 017123
[35] Fano U 1961 *Phys. Rev.* **124** 1866